Supporting Information for "Plasmon-driven sub-picosecond breathing of metal nanoparticles"

Franco P. Bonafé, Bálint Aradi, Mengxue Guan, Oscar A. Douglas-Gallardo, Chao Lian, Sheng Meng, Thomas Frauenheim and Cristián G. Sánchez

July 25, 2017

S1 Non-adiabatic forces

In DFTB the force has three main contributions: the band, coulombic and repulsive components:

$$F_A = -\mathrm{Tr}\left(\rho\left[\nabla_A H\right]\right) - \nabla_A\left[\sum_{BC}\gamma_{BC}\Delta q_B \Delta q_C\right] - \nabla_A E_{rep}$$

which after replacing by the expression for the hamiltonian and calculating the gradients considering a non-orthogonal basis, leads to:

$$F_A = -\mathrm{Tr}\left[\rho\left(\nabla_A H + \nabla_A S\sum_C \gamma_{AC}\Delta q_C - \frac{1}{2}\left(\nabla_A S S^{-1} H + H S^{-1}\nabla_A S\right)\right)\right] - \nabla_A E_{rep} - \Delta q_A \sum_B \nabla_A \gamma_{AB}\Delta q_B$$

where ρ is the instantaneous density matrix, H is the self-consistent hamiltonian, S is the overlap matrix, q_A is the charge of atom A, E_{rep} is the repulsive energy and γ_{AB} is a function of the interatomic distance.

S2 Absorption spectra

Absorption spectra were obtained using the real-time propagation approach as described in the manuscript, and are shown in Figure S1. TDDFT was used to compute only the spectrum of the Ag_{55} nanoparticle due to computational limitations. The TDDFT spectrum and plasmon energy show remarkable agreement with the experimental measurement published in Phys. Chem. Chem. Phys. 17, 17541-17544, 2015.

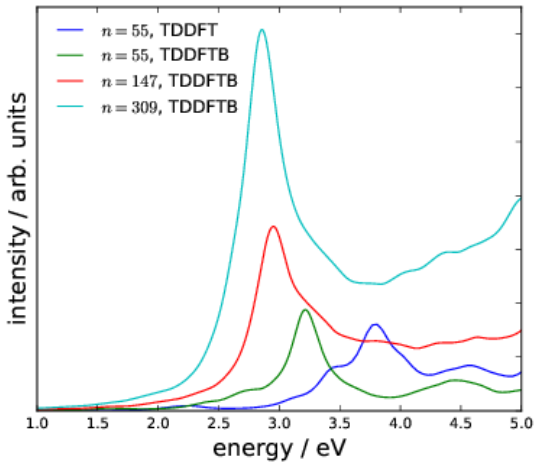

Figure S1: Absorption spectra obtained using different methodologies.

S3 Comparison of the pulse envelope shape

The pulses used for both TDDFT and TDDFTB simulations are different in shape (Gaussian and Sin^2) and total width (25 and 40 fs). As shown in Figure S2, the oscillation frequency does not change and only a change in amplitude for the longer pulse (Gaussian) is observed. As the responses of both systems were analyzed focusing on the frequency, while the amplitudes were only compared qualitatively, this difference was not relevant for the discussion and main conclusions of our work.

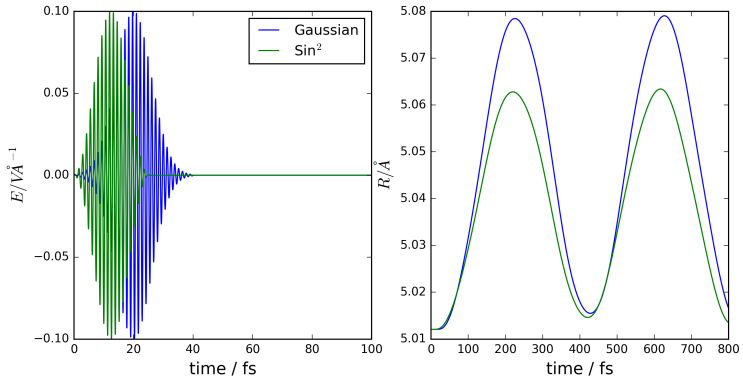

Figure S2: Pulse shape (left) and radius vs. time responses (right) for both pulses used in our work.

S4 Results for several field intensities

In Figure S3 the radius is plotted as a function of time for several field intensities of the 25-fs pulse. Frequency of the pulse is always resonant with the plasmon mode. It is easy to note the existence of three regimes: fields smaller than a threshold value of approx. 0.1 VÅ^{-1} in which the oscillation frequency is not always consistent with the quasi-breathing mode (QBM) period, and the oscillations are very small in amplitude and almost undetectable in the animations; a quasi-harmonic regume between 0.1 VÅ^{-1} and 0.5 VÅ^{-1}, with increasing amplitude as the field increases; and a photo-fragmentation regime, for intensities higher than 0.5 VÅ^{-1}, in which depending on the particle size it melts or breaks down into fragments, up to the limit of complete photoatomization (not shown in the figure) for fields higher than 1.0 VÅ^{-1}.

Figure S4 depicts the change in temperature, calculated from the kinetic energy as shown in equation 1. The reader should keep in mind that particles are initially at rest, as the initial temperature is zero, the mean temperature is equal to the mean temperature change. This value increases with the field intensity as it can be seen in Figure S5.

$$T_{ave} = \frac{2}{3k_B n} E_{kin} \tag{1}$$

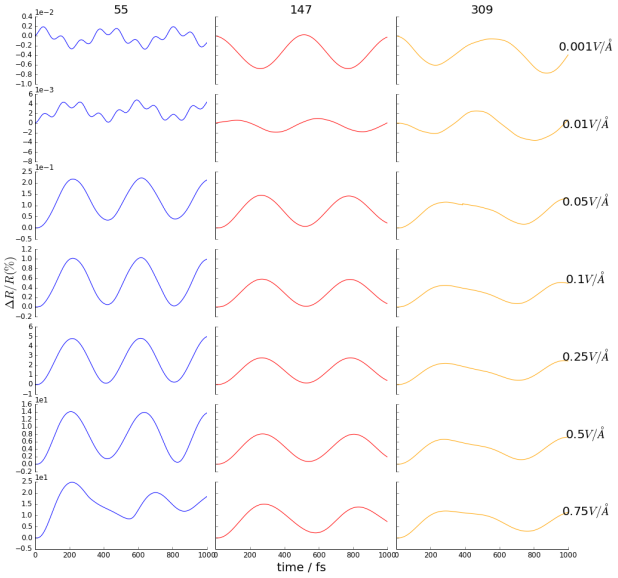

Figure S3: Average radius as a function of time for the three nanoparticle sizes considered in this work and several field intensities.

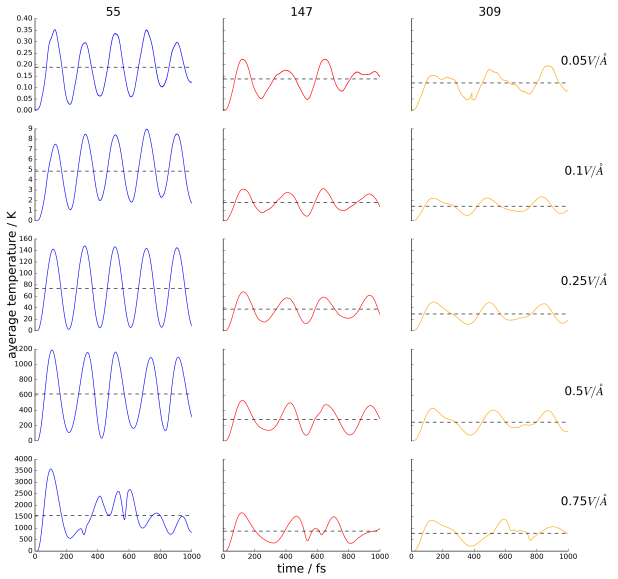

Figure S4: Temperature as a function of time for different sizes and several field intensities. Average temperature is represented with dashed horizontal lines.

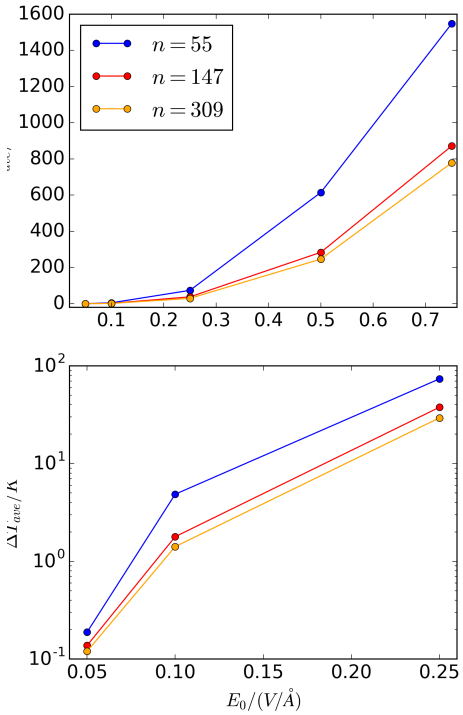

Figure S5: Top: mean temperature change as a function of field intensity for different sizes. Bottom: the same considering the three field intensities considered for Figure 2 of the article, and using a log scale in the y axis.

S5 Orbital populations versus time

The change of the population of the states, projected on the initial (ground state) orbitals, is shown in Figure S6 as a function of time and orbital energy, similar to the plot in Figure 4 of the main paper. Even when it is evident that the electrons remain excited after the pulse for the short times considered here, it is enough evidence that electron-phonon coupling is not the cause for the oscillations since in all cases oscillations are launched before the first 100 fs of the simulation.

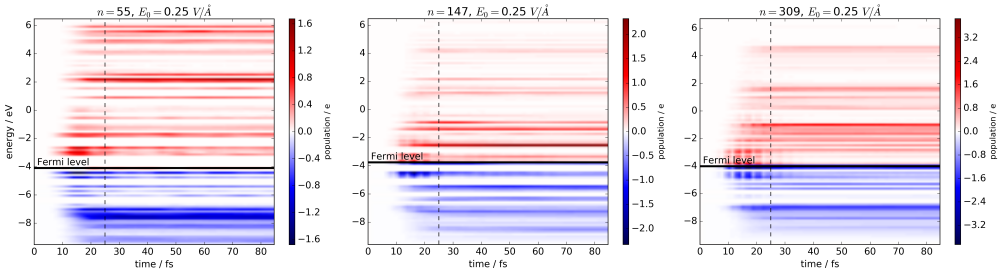

Figure S6: Change of populations projected on ground state orbitals vs. time and orbital energy, for the $n = 55$ (left), $n = 147$ (middle) and $n = 309$ (right) nanoparticles.

S6 Oscillation parameters

The evolution of the average NP radius vs. time was fitted to sin functions with four parameters, as shown in equation 2, where: R_0 is the (new) equilibrium radius, ϕ is the phase (in radians), and A and T are the oscillation amplitude and period, respectively. The original and fitted curves are shown in Figure S7. The parameters as a function of field intensity E_0 are plotted and analyzed in Figure S8. As it is claimed in the main text, the period and phase don't show significant dependence on the external field, while the amplitude and change in equilibrium radius increase proportionally to the field leading to the scaling laws described in the paper.

$$R = R_0 + A \sin\left(2\pi \frac{t}{T} + \phi\right) \tag{2}$$

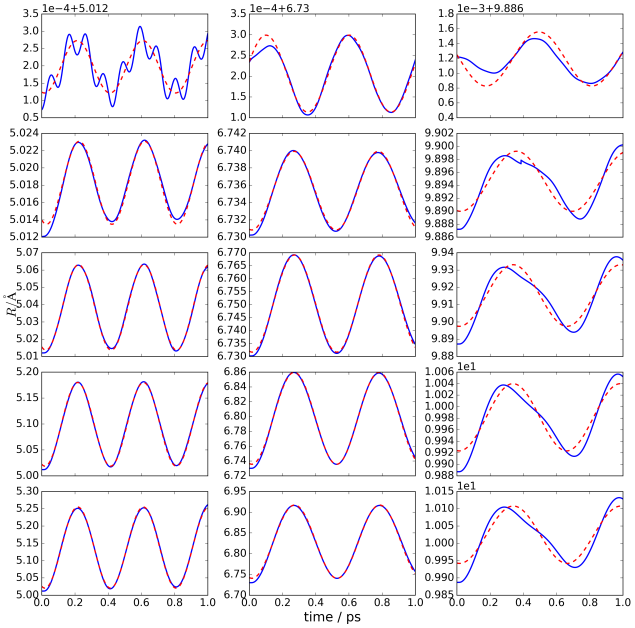

Figure S7: Fitting of sin functions for $n = 55$ (left), $n = 147$ (middle) and $n = 309$ (right) nanoparticles, for field values of (from top to bottom) 0.01, 0.05, 0.1, 0.2 and 0.25 VÅ^{-1} respectively.

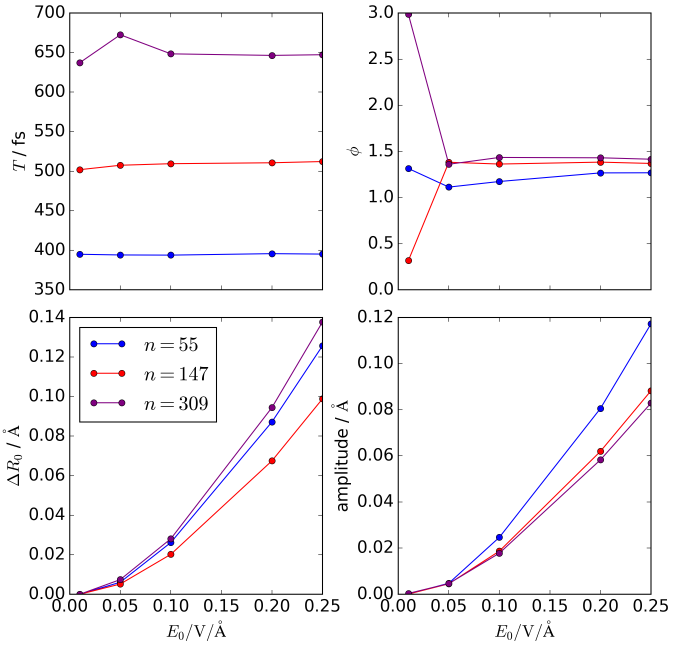

Figure S8: Fitted parameters as a function of field intensity.